Coherent frequency mixing in microparticle composites

T. P. Shen and D. Rogovin
Rockwell International Science Center, Thousand Oaks, California 91360
(Received 12 October 1989)

We examine coherent sum and difference-frequency generation in dilute suspensions of metallic or *n*-type semiconductor microspheres embedded in a passive linear dielectric host using quasihydrodynamic theory within the quasistatic and single-scattering approximations. If one or both of the incident laser-beam frequencies are near the surface dipole resonance, the medium exhibits an enhanced response. Enhancement of the sum-frequency wave is also possible if this frequency coincides with the surface quadrupole resonance of the microsphere. It is shown that a coherent second-order response is possible only if the symmetry of the system is reduced. Detailed calculations are presented for the dynamic response of the individual particles as well as the macroscopic electrodynamics of the composite as a whole. Numerical results for the perturbed electron density and drift velocity as well as the laser-induced, microparticle quadrupole moment of a single microsphere are displayed. Numerical results for the coherent and incoherent intensities are calculated for a 1-mm-thick slab of microparticles embedded in an artificial glass host. The microparticles are silver spheres of 100 Å radius with 10^{-4} volume fraction. The coherent intensity for a mm-thick microparticle composite is nonvanishing only for a noncollinear configuration under perfect phase matching. If both of the incident laser-beam frequencies are near the surface dipole resonances, the conversion efficiencies of the coherent (incoherent) radiation at the sum and difference frequencies are 10^{-6} (10^{-7}) and 10^{-11} (10^{-16}), respectively. The conversion efficiencies for the sum-frequency generation at the surface quadrupole resonance are 10^{-7} and 10^{-10} for the coherent and incoherent intensities.

I. INTRODUCTION

There has been considerable interest in the nonlinear electrodynamical characteristics of microparticle composites.[1] Of particular interest are situations in which one or more of the microparticle's Fröhlich modes has been resonantly excited by incident laser light. For such situations excitation of this surface mode amplifies the incident laser intensity, which gives rise to enhanced nonlinear optical coefficients.[2]

Here, the coherent generation of sum- and difference-frequency radiation from a microparticle composite is examined using quasihydrodynamic theory.[3] There are a number of motivations for focusing on this problem. Hua and Gersten[4] examined incoherent second-harmonic generation from composites of microparticles, and it is natural to extend their calculations to a more general situation. Furthermore, because of symmetry, a coherent response is not possible at the second harmonic if the medium is irradiated by a single laser beam. Thus the only nonlinear response to a single laser in second order of perturbation theory is incoherent scattering at the second-harmonic frequency. Since the efficiency for this process is low, it is difficult to perform an experiment to validate the theory, whereas the more efficient coherent sum-frequency generation may be observable. In addition, beam combination via nondegenerate two-wave mixing (NDTWM) involves the nonlinear response of the composite to two laser beams operating at different wavelengths. Hence sum- and difference-frequency wave generation are intermediate processes to NDTWM and serve as a useful step for understanding beam combination in a microparticle composite.

This paper is divided into four parts, of which this, the introductory part, is the first. In the Sec. II, the problem is formulated in terms of the perturbative response of a particle, which consists of a degenerate electron gas moving in a positive uniform jellium background, to two laser beams within the quasihydrodynamic approximation.[3] We extract the second-order dynamic response of the particle to laser light. Specifically, we determine the perturbed electron density and drift velocity as well as the laser-induced quadrupole moment associated with the sum- and difference-frequency waves. The electrodynamic properties of the local fields in the vicinity of the microparticles are also resolved. Section III is concerned with the macroscopic electrodynamic response of the medium, as a whole, and results are presented for the intensity, polarization, and angular dependence of the coherent sum- and difference-frequency waves emitted by the composite in the presence of two noncollinear laser beams. In the collinear limit, no coherent sum- or difference-frequency wave is emitted by the composite as in second-harmonic generation. We evaluate the surface-enhanced, second-order optical susceptibilities associated with sum- and difference-frequency wave generation in the noncollinear configuration. The composite always produces sum- and difference-frequency radiation via incoherent, nonlinear scattering processes, and the physical characteristics of this radiation are examined. In Sec. IV, we present numerical results for a silver microsphere composite and discuss our findings. Mathematical details are given in the appendixes.

II. FORMULATION

We consider a metallic or n-type semiconductor microparticle composite whose particle size is less than 100 Å. This is small compared to any of the radiation wavelengths so that the Rayleigh limit is valid. Also, the quasistatic approximation is used where the Maxwell equations are reduced to the electrostatic equation. We note that Fuchs and Kliewer have shown that the hydrodynamic and self-consistent field approximations yield the same results at all experimentally accessible frequencies.[5] Thus Landau damping can be accounted for with a simple dissipation model characterized by a frequency-independent damping constant ν. We also assume that microparticle size exceeds 20 Å so that the quantum-size effect is not important.[6] If the incident and nonlinear-generated frequencies are all sufficiently high, the ionic (or phonon) contribution inside the microparticles will be negligible. We can assume that each of the microparticles in the composite consists of a rigid, positive jellium background with charge density en_0 accompanied by a degenerate electron gas. Charge neutrality demands that the unperturbed electron density be n_0, and in the presence of laser radiation the perturbed electron density is denoted by $n(\mathbf{r},t)$. The hydrodynamic equations, which are the Euler equation and the equation of continuity, govern the response of the electron gas to incident laser radiation. Here, we examine the second-order response of a single sphere, which consists of a degenerate electron gas, confined to a microsphere of radius a, embedded in a passive linear dielectric and irradiated by two laser beams, operating at frequencies ω_1 and ω_2. The unperturbed electron profile is taken to be a step function. Although a step function does poorly for a flat metal surface,[7] we adopt it here for several reasons. (1) It is the standard model used for modeling the nonlinear optics due to the resonant plasmon responses of metallic microspheres[4] and, using more complex spatial profiles, is computationally prohibitive. (2) The nonlinear plasmon response appears to involve the electron fluid deep within the microsphere, not just at the surface. Thus, on physical grounds, the frequency-mixing properties of these resonances should not be overly sensitive to the details of the electron profile near the surface. Mathematically, this is reflected in the fact that the quadrupole moment requires an integration of various moments of the density over the entire volume of the microsphere. (3) Although other profiles will give different results, these differences are masked by the fact that numerous suspension parameters (geometric shape, particle size distribution, and metallic purity) will vary significantly from the model and from sample to sample.

The physical situation is depicted in Fig. 1. The ω_1 beam is incident normal to the surface of microparticle composite, is linearly polarized in the z direction, and has propagation vector $\mathbf{k}_1=k_1\hat{\mathbf{x}}$ within the medium. The second laser beam is oriented at an angle θ_2 with respect to the first beam, and has a unit polarization vector $\hat{\mathbf{e}}_2=(\hat{\mathbf{x}}\cos\theta_2+\hat{\mathbf{z}}\sin\theta_2)$ and a propagation vector $\mathbf{k}_2=k_2(\hat{\mathbf{x}}\sin\theta_2-\hat{\mathbf{z}}\cos\theta_2)$ within the medium. Here, $k_j=[\epsilon_h(\omega_j)]^{1/2}\omega_j/c$, with $\epsilon_h(\omega_j)$ the dielectric constant

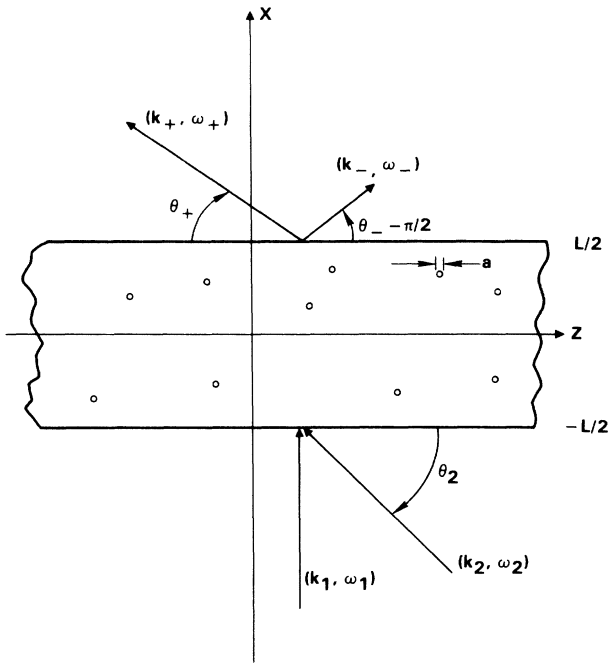

FIG. 1. System to be considered.

of the host at the frequency ω_j.

Within each microparticle, laser radiation induces an electron drift velocity $\mathbf{v}(\mathbf{r},t)$ whose dynamics is governed by the Euler equation

$$n(\mathbf{r},t)\left[\frac{\partial}{\partial t}+\nu+\mathbf{v}(\mathbf{r},t)\cdot\nabla\right]\mathbf{v}(\mathbf{r},t) = -en(\mathbf{r},t)\mathbf{E}(\mathbf{r},t)/m-\nabla p(\mathbf{r},t)\ . \quad (2.1)$$

Here, ν is the electron collision frequency and $p(\mathbf{r},t)$ is the quantum pressure of the degenerate electron gas, which within the Thomas-Fermi approximation[3] is given by

$$p(\mathbf{r},t)=\left[\frac{3}{8\pi}\right]^{2/3}\left[\frac{\hbar^2}{5m}\right]n(\mathbf{r},t)^{5/3}\ . \quad (2.2)$$

The third term on the left-hand side (lhs) of the Euler equation is the convective current, which arises from the fact that the conduction electrons are a continuous medium in this model. The first term on the right-hand side (rhs) of Eq. (2.1) is the Lorentz force, the magnetic term having been dropped within the electrostatic approximation. The last term is due to quantum pressure, which gives rise to a spatial variation (i.e., a screening) in the electron density near the microparticle surface in the presence of radiation. Thus the response of the electron gas is nonlocal. The perturbed electron charge density $n(\mathbf{r},t)$ obeys the equation of continuity:

$$\frac{\partial n(\mathbf{r},t)}{\partial t}+\nabla\cdot[n(\mathbf{r},t)\mathbf{v}(\mathbf{r},t)]=0\ . \quad (2.3)$$

The incident electric component of the laser radiation field $\mathbf{E}_0(\mathbf{r},t)$ is given by

$$\mathbf{E}_0(\mathbf{r},t)=\mathbf{e}_1 A_1\exp[i(\mathbf{k}_1\cdot\mathbf{r}-\omega_1 t)] + \mathbf{e}_2 A_2\exp[i(\mathbf{k}_2\cdot\mathbf{r}-\omega_2 t)]+\text{c.c.} , \quad (2.4)$$

where $\mathbf{e}_j$, A_j, $\mathbf{k}_j$, and $\omega_j (j=1,2)$ are the incident unit polarization vector, electric field amplitude, wave vector, and frequency of the jth laser beam. The total electric field amplitude $\mathbf{E}(\mathbf{r},t)$ in Eq. (2.1) is driven by the perturbed charge density inside the microparticle. Within the quasistatic approximation, we have $\mathbf{E}(\mathbf{r},t) = -\nabla\Phi(\mathbf{r},t)$, where $\Phi(\mathbf{r},t)$ is the electrostatic potential. Outside the microparticle, the Laplace equation holds:

$$\nabla^2\Phi(\mathbf{r},t)=0 . \quad (2.5a)$$

Inside the microsphere, the electrostatic potential obeys Poisson's equation:

$$\nabla^2\Phi(\mathbf{r},t)=4\pi e n(\mathbf{r},t)/\epsilon_b , \quad (2.5b)$$

where the electrostatic potential is coupled to Eqs. (2.1) and (2.3) via $n(\mathbf{r},t)$, and ϵ_b is the dielectric constant of the rigid jellium background. Equations (2.5) must be supplemented with the usual electrostatic boundary conditions, namely, that $\Phi(\mathbf{r},t)$ and $\epsilon\partial\Phi(\mathbf{r},t)/\partial r$ are continuous at the surface. Since the Euler equation and the equation of continuity are coupled together, we require only one additional boundary condition (ABC), which is usually chosen to be the acoustic condition to ensure no electrons flow across the boundary; viz., the radial component of the electron drift velocity will vanish at the surface. These boundary conditions can be followed without any difficulties in determining the linear response of the microparticle to laser light. However, in the next order of perturbation theory, difficulties can arise in the presence of the monopole response.[4] Specifically, if one demands that the second-order radial velocity vanish at the microparticle's surface, then the integral of the second-order perturbed electron density over the volume of the microparticle will deviate from zero. In turn, this implies that the calculation does not conserve charge and reflects the fact that there are basic inconsistencies in describing the microparticle response by means of a relaxation model.[8] Here, we use a different additional boundary condition for monopole responses, namely, that the charge is conserved in every order of perturbation theory. If this is done, then the second-order radial velocity will deviate from zero at the microparticle's surface. Calculations in Sec. IV will show that within a screening length of the surface, the ratio of the radial velocity at the surface to the maximum velocity is of order $\nu/\omega_\pm$, where $\omega_\pm$ is the frequency of the radiation generated by the microparticle via nonlinear mixing processes. Thus, so long as $\nu/\omega_\pm \ll 1$, this inconsistency is not significant.

An examination of Eqs. (2.1) and (2.2) reveals that there are four nonlinear terms in the Euler equation for the electron drift velocity: (1) the electron current, (2) the convective current, (3) the Lorentz force, and (4) the quantum pressure.

The electron density, drift velocity, quantum pressure, and the electrostatic potential can be decomposed into the different possible frequency components. Thus, if $\alpha(\mathbf{r},t)$ is any of these quantities, we have

$$\alpha(\mathbf{r},t)=\alpha_0+\alpha_1(\mathbf{r},\omega_1)\exp(-i\omega_1 t) + \alpha_1(\mathbf{r},\omega_2)\exp(-i\omega_2 t)+\alpha_2(\mathbf{r},\omega_-)\exp(-i\omega_- t) + \alpha_2(\mathbf{r},\omega_+)\exp(-i\omega_+ t)+\text{c.c.} , \quad (2.6)$$

where α_0 is the equilibrium value. In Eq. (2.6), we need to include only the sum- ($\omega_+=\omega_1+\omega_2$) and difference- ($\omega_-=\omega_1-\omega_2$) frequency terms for the second-order response. In the limit that $\omega_1\to\omega_2$, the difference-frequency term becomes a rectified correction and the sum-frequency term contributes to the second-harmonic response.

A. Linear response

Inserting the perturbative expansion, i.e., Eq. (2.6), into Eqs. (2.1)–(2.5), we find that the induced linear density satisfies the following equation:

$$[\nabla^2-q^2(\omega)]n_1(\mathbf{r},\omega)=0 . \quad (2.7a)$$

In Eq. (2.7a), $q(\omega)$ is the self-consistent, frequency-dependent screening wave vector, which is given by

$$q(\omega)=[\omega_p^2-\omega(\omega+i\nu)]^{1/2}/\beta , \quad (2.7b)$$

where $\omega_p=(4\pi n_0 e^2/m\epsilon_b)^{1/2}$ is the plasma frequency and $\beta^2=0.6v_F^2$, with v_F the Fermi velocity. In the low-frequency limit, the screening wave vector becomes real and reduces to the Thomas-Fermi value $q_{\rm TF}=\omega_p/\beta$. In this limit, the field barely penetrates into the particle and the electron density is uniform everywhere, except in the immediate vicinity of the particle's surface. In the high-frequency limit, i.e., $\omega\geq\omega_p$, $q(\omega)$ has an imaginary part and the electron density is oscillatory. Explicit expressions for the first-order electron density and electric field, as well as the drift velocity are given in Appendix A.

B. Quadratic response

To determine the quadratic response of the electron gas to two nondegenerate laser beams oscillating at ω_1 and ω_2, we insert the expressions for the linear electron density, drift velocity, and electric field into Eqs. (2.1) and (2.3), and extract out those terms that are oscillating at $\omega_\pm$ for sum- (ω_+) and difference- (ω_-) frequency generation. This leads to the following equation for the second-order electron density response oscillating at $\omega_\pm$:

$$[\nabla^2-q^2(\omega_\pm)]n_2(\mathbf{r},\omega_\pm)=-\beta^{-2}\nabla\cdot\mathbf{S}(\mathbf{r};\omega_1,\pm\omega_2) , \quad (2.8)$$

where the drive terms $\mathbf{S}(\mathbf{r};\omega_1,\pm\omega_2)$ are defined by

$$\mathbf{S}(\mathbf{r};\omega_1,\pm\omega_2)=i\omega_1 n_1(\mathbf{r},\omega_1)\mathbf{v}_1(\mathbf{r},\pm\omega_2)\pm i\omega_2 n_1(\mathbf{r},\omega_1)\mathbf{v}_1(\mathbf{r},\pm\omega_2)+n_0[\mathbf{v}_1(\mathbf{r},\omega_1)\cdot\nabla]\mathbf{v}_1(\mathbf{r},\pm\omega_2)+n_0[\mathbf{v}_1(\mathbf{r},\pm\omega_2)\cdot\nabla]\mathbf{v}_1(\mathbf{r},\omega_1) + e/m[n_1(\mathbf{r},\omega_1)\mathbf{E}_1(\mathbf{r},\pm\omega_2)+n_1(\mathbf{r},\pm\omega_2)\mathbf{E}_1(\mathbf{r},\omega_1)]+(2\beta^2/3n_0)\nabla[n_1(\mathbf{r},\omega_1)n_1(\mathbf{r},\pm\omega_2)] . \quad (2.9)$$

The linear response $n_1(\mathbf{r},\omega)$, $\mathbf{v}_1(\mathbf{r},\omega)$, and $\mathbf{E}_1(\mathbf{r},\omega)$ are all enhanced at the surface-mode frequencies ω_S. The drive term $\mathbf{S}(\mathbf{r};\omega_1,\pm\omega_2)$ may be doubly enhanced for ω_1 and ω_2 near ω_S, since $\mathbf{S}(\mathbf{r};\omega_1,\pm\omega_2)$ is a bilinear product of linear responses at ω_1 and ω_2. For compact notation, we shall denote $\mathbf{S}(\mathbf{r};\omega_1,\pm\omega_2)$ as $\mathbf{S}_\pm(\mathbf{r})$. The first two terms in $\mathbf{S}_\pm(\mathbf{r})$ arise from the second-order electron current, the next two are from the second-order convective current, the fifth and sixth terms arise from the second-order Lorentz force, while the last term arises from the second-order quantum pressure. The explicit expression for the drive terms are given by

$$\mathbf{S}_\pm(\mathbf{r})=\frac{\Gamma_\pm\beta^2}{q_\pm a}[\hat{\mathbf{r}}S_r^\pm(r)+\hat{\boldsymbol{\theta}}S_\theta^\pm(r)+\hat{\boldsymbol{\phi}}S_\theta^\pm(r)] , \tag{2.10}$$

with

$$S_r^\pm(r)=(4\pi/9)^{1/2}S_{r_{00}}^\pm(r)\sin\theta_2 Y_{00}(\theta) +(16\pi/45)^{1/2}S_{r_{20}}^\pm(r)\sin\theta_2 Y_{20}(\theta) -(2\pi/15)^{1/2}S_{r_{21}}^\pm(r) \times\cos\theta_2[Y_{21}(\theta,\phi)-Y_{2-1}(\theta,\phi)] , \tag{2.11a}$$

$$S_\theta^\pm(r)=-\tfrac{1}{2}S_{\theta_{20}}^\pm(r)\sin\theta_2\sin2\theta +[S_{\theta C}(r,\omega_1,\pm\omega_2)\cos^2\theta -S_{\theta S}(r,\omega_1,\pm\omega_2)\sin^2\theta]\cos\theta_2\cos\phi , \tag{2.11b}$$

$$S_\phi^\pm=-S_{\phi_{21}}^\pm(r)\cos\theta_2\cos\theta\sin\phi , \tag{2.11c}$$

where the different components $S_{\mu_{lm}}^\pm(r)$ are given in Eqs. (B1). Explicit expressions for the second-order electric field as well as the electron density and velocity are contained in Appendix B.

III. MACROSCOPIC ELECTRODYNAMIC RESPONSE

In this section, we determine the macroscopic second-order electromagnetic response of a very dilute microparticle composite to two different lasers operating at frequencies ω_1 and ω_2 within the single scattering approximation. The first step is to determine the radiation field in the far zone due to a single microparticle using the results obtained in Sec. II. The total field, which is generated by the entire composite, can be obtained by summing up the contribution of each particle.

A. Scattering amplitude and the radiation field in the far zone

In this section, we determine the second-order electromagnetic fields in the radiation zone, which are generated by a single microsphere. A microsphere at point $\mathbf{r}'=(x',y',z')$ scatters the two incident beams, to generate a second-order field $\mathbf{E}_s(\mathbf{r},\omega_\pm)$ at the sum (ω_+) or difference (ω_-) frequency at point $\mathbf{r}=(x,y,z)$, where $r\gg a$ in the radiation zone. The electromagnetic field associated with an oscillating quadrupole of the microsphere located at $\mathbf{r}'$ is given by

$$\mathbf{E}_s(\mathbf{r},\mathbf{r}',\omega_\pm)=\exp[i\phi(\mathbf{r},\mathbf{r}')]\mathbf{f}_\pm(\theta',\phi')/|\mathbf{r}-\mathbf{r}'| , \tag{3.1}$$

where the phase $\phi(\mathbf{r},\mathbf{r}')$ is given by

$$\phi(\mathbf{r},\mathbf{r}')=k_\pm|\mathbf{r}-\mathbf{r}'|+(\mathbf{k}_1\pm\mathbf{k}_2)\cdot\mathbf{r}' , \tag{3.2}$$

and $k_\pm=[\epsilon_h(\omega_\pm)]^{1/2}\omega_\pm/c$ the integration is over the volume $V'=(4\pi/3)a^3$ of the sphere at $\mathbf{r}'$. In the quasi-static limit where the radiation wavelength $\lambda\gg a$, the phase factors in Eq. (3.2) remain nearly constant within a given sphere. Hence the scattering amplitude in Eq. (3.1) is given by

$$\mathbf{f}_\pm(\theta',\phi')=-i(k_\pm^3/2)[\mathbf{n}\times\mathbf{Q}(\mathbf{n})/3]\times\mathbf{n} , \tag{3.3}$$

where the vector $\mathbf{Q}(\mathbf{n})$ is defined by

$$Q_\mu(n_\nu)=\sum_{\mu,\nu}Q_{\mu\nu}n_\nu . \tag{3.4}$$

$Q_{\mu\nu}$ is the second-order quadrupole moment tensor induced by the laser light in a microparticle located at the origin, $\cos\theta'=(z-z')/r$ and $\tan\phi'=(y-y')/(x-x')$. Note that the quadrupole moment tensor $\mathbf{Q}$ can be extracted from the electrostatic field in the near zone for a small scatter. For a microsphere irradiated by two laser beams oriented at an angle of θ_2 with respect to each other, the radiation-induced quadrupole moment tensor is given by

$$Q=\begin{pmatrix}0&0&Q_{xz}\\0&0&0\\Q_{zx}&0&Q_{zz}\end{pmatrix} , \tag{3.5}$$

where $Q_{\mu\nu}=Q_{\nu\mu}$. Explicit formulas for $Q_{\mu\nu}$ are given in Eqs. (B17). Finally, the scattering amplitude $\mathbf{f}_\pm(\theta',\phi')$, for the electric field in the radiation zone, arising from a single microparticle is

$$\mathbf{f}_\pm(\theta',\phi')=ik_\pm^3a^5\{2\pi e\Gamma_\pm/[3\epsilon_h(\omega_\pm)+2\epsilon_b]\}\{\hat{\boldsymbol{\theta}}[-\sin\theta_2\sin2\theta'U_{20}^\pm/2+\cos\theta_2\cos2\theta'\cos\phi U_{21}^\pm] -\hat{\boldsymbol{\phi}}\cos\theta_2\cos\theta'\sin\phi'U_{21}^\pm\} . \tag{3.6}$$

Note that in collinear limit ($\theta_2=\pi/2$), the scattering amplitude has a component only in the θ direction. The functions $U_{lm}^\pm$ are dimensionless, are related to weighed averages of the various components of the charge density over the sphere, and are defined in Appendix B.

The magnetic field components $\mathbf{B}_s(\mathbf{r},\mathbf{r}',\omega_\pm)$ are then given by

$$\mathbf{B}_s(\mathbf{r},\mathbf{r}',\omega_\pm)=\mathbf{n}\times\mathbf{E}_s(\mathbf{r},\mathbf{r}',\omega_\pm) , \tag{3.7}$$

so that the total intensity $I_s(\mathbf{r},\mathbf{r}',\omega_\pm)$, for a single microparticle at $\mathbf{r}'$ is

$$I_s(\mathbf{r},\mathbf{r}',\omega_\pm)=(c/8\pi)|\mathbf{f}_\pm(\theta',\phi')|^2/|\mathbf{r}-\mathbf{r}'|^2 , \tag{3.8}$$

where $\mathbf{f}_\pm$ is defined in Eq. (3.3).

B. Macroscopic electromagnetic fields and intensities

In this section, we examine the total electromagnetic fields and intensities arising from a tenuous collection of microparticles randomly distributed in a passive linear dielectric host. In general, a collection of microparticles will scatter radiation with random phase with respect to one another. The resultant total electromagnetic field from a microparticle composite will be the sum of the coherent (or average) field and the incoherent (fluctuating) field.[9] The phase of the field will fluctuate randomly for arbitrary directions, so that the volume-averaged (or ensemble-averaged) incoherent field is zero. However, along a particular phase-matched (or coherent) direction, the different particles all scatter in phase with one another and the resultant average field is coherent. This coherent field will be discussed in Sec. III B 1. The average intensity for a microparticle composite is the sum of the coherent and incoherent intensities, and will be examined in Sec. III B 2. We will consider a tenuous microsphere composite with the particles sufficiently far apart so that they do affect each other. Then, the far-field and single scattering approximations are valid, and the total field at a point $\mathbf{r}$ is the sum of the far field from each microsphere located at point $\mathbf{r}'$, as depicted in Fig. 1.

1. Coherent field

The coherent field at $\omega_\pm$ is given by the integral (or summation) of the far field of each sphere, which is given in Eq. (3.1), over the entire composite, i.e.,

$$\mathbf{E}_c(\mathbf{r},\omega_\pm)=\int_v d\mathbf{r}'\,\mathbf{E}_s(\mathbf{r},\mathbf{r}',\omega_\pm) , \tag{3.9a}$$

$$=N\int_{-1/2L}^{1/2L}dx'\int_{-1/2L_y}^{1/2L_y}dy'\int_{-1/2L_z}^{1/2L_z}dz'\exp[i\phi(\mathbf{r},\mathbf{r}')]\mathbf{f}_\pm(\theta',\phi')/|\mathbf{r}-\mathbf{r}'| , \tag{3.9b}$$

where the composite is assumed to reside within a slab of dimensions $L\times L_y\times L_z$, where $L\ll L_y,L_z$ and $L_yL_z\to\infty$, but L remains finite and N is the microsphere number density. The prefactors, which include the scattering amplitude $\mathbf{f}_\pm$ and the propagator $1/|\mathbf{r}-\mathbf{r}'|$, vary slowly with $\mathbf{r}'$ in comparison to the rapidly varying exponential factor $\exp[i\phi(\mathbf{r},\mathbf{r}')]$. We are concerned with the limiting case in which $r\gg L$. To evaluate the integral for the y' and z' coordinate first for the slab, we will use the method of steepest descents.[9] The stationary phase point for the microsphere is located at $\mathbf{r}_\pm=(r_\pm,\theta_\pm,\phi_\pm)$, which are

$$r_\pm=|x-x'|/\sin\theta_\pm , \tag{3.10a}$$

$$\phi_\pm=0 , \tag{3.10b}$$

$$\cos\theta_\pm=\pm k_2\cos\theta_2/k_\pm , \tag{3.10c}$$

and $\theta_\pm$ are the coherent angles at $\omega_\pm$. An examination of Eq. (3.10c) reveals that there is always a stationary phase point for the sum-frequency (ω_+) wave or the difference-frequency (ω_-) wave, if $k_\pm>k_2\cos\theta_2$. Thereby it restricts the range of angles in which the second laser can be aligned for coherent sum- or difference-frequency wave generation.

The last integral over the x' coordinate in Eq. (3.8b) is over a finite region and will give rise to the phase-matching term. Then, the coherent field in Eq. (3.8) is given by

$$\mathbf{E}_c(\mathbf{r},\omega_\pm)=\hat{\mathbf{r}}_\pm pLj_0(\Delta_\pm L/2)f_\pm(\theta_2|\theta_\pm,0)\times\left[\frac{2\pi i}{k_\pm\sin\theta_\pm}\right]\exp[i\Delta_\pm L/2+i\phi_\pm(\mathbf{r})] , \tag{3.11}$$

where unit polarization vector of the coherent electric field at point $\mathbf{r}$ far outside the slab is $\hat{\mathbf{r}}_\pm=\hat{\mathbf{x}}\cos\theta_\pm-\hat{\mathbf{z}}\sin\theta_\pm$, $j_0(z)=\sin z/z$ is the usual phase-matching term, and $p=N4\pi a^3/3$ is the volume fraction of microspheres. In Eq. (3.11), the scattering amplitude per unit volume $f_\pm$ is evaluated at the stationary phase point and is given by

$$f_\pm(\theta_2|\theta_\pm,0)=i\tfrac{3}{2}e\Gamma_\pm k_\pm^3a^2[\cos\theta_2\cos2\theta_\pm U_{21}^\pm+\tfrac{2}{3}\sin\theta_2\sin2\theta_\pm U_{20}^\pm]/[3\epsilon_h(\omega_\pm)+2\epsilon_b] , \tag{3.12}$$

while the phase of the wave $\phi_\pm(\mathbf{r})$ is

$$\phi_\pm(\mathbf{r})=k_\pm[\sin\theta_\pm x+\cos\theta_\pm z] . \tag{3.13}$$

The phase factor $\Delta_\pm L/2$ arises from phase mismatch between the polarization driven by incident waves and nonlinear wave, which is given by

$$\Delta_\pm=k_1+k_2\sin\theta_2-k_\pm\sin\theta_\pm . \tag{3.14}$$

An examination of the scattering amplitude evaluated at the stationary phase point reveals that there is no coherent response if the lasers are collinear, viz., $\theta_2=\pi/2=\theta_\pm$.

2. Total intensity

The total intensity for the sum- and difference-frequency generation from a slab of microparticle composite of thickness L is given by

$$I(\mathbf{r},\omega_\pm)=N\int_{-1/2L}^{1/2L}dx'\int_{-\infty}^{\infty}dy'\int_{-\infty}^{\infty}dx' I_s(\mathbf{r},\mathbf{r}',\omega_\pm)\ , \tag{3.15}$$

where N is the microparticle number density and I_s is given in Eq. (3.8). The total intensity can be decomposed into two parts, viz., the coherent and incoherent intensities. The coherent part is given by

$$I_c(\mathbf{r},\omega_\pm)=\frac{c}{8\pi}\mathbf{E}_c(\mathbf{r},\omega_\pm)\times\mathbf{B}_c(\mathbf{r},\omega_\pm)\cdot\hat{\mathbf{r}}\ , \tag{3.16a}$$

$$=p^2L^2\frac{9\pi c}{8}\frac{|k_\pm|^4a^4e^2|\Gamma_\pm|^2}{|3\epsilon_h(\omega_\pm)+2\epsilon_b|^2}i_c^\pm(\theta_2)\times|j_0(\Delta_\pm L/2)|^2\ , \tag{3.16b}$$

where

$$i_c^\pm(\theta_2)=|\cos\theta_2\cos2\theta_\pm U_{21}^\pm+\tfrac{2}{3}\sin\theta_2\sin2\theta_\pm U_{20}^\pm|^2\ , \tag{3.16c}$$

$\mathbf{B}_c=\hat{\mathbf{r}}\times\mathbf{E}_c$, and $\mathbf{E}_c$ is given in Eq. (3.11). The incoherent part is given by

$$I_i(\mathbf{r},\omega_\pm)=\frac{c}{8\pi}N\int_{-1/2L}^{1/2L}dx'\int_{-\infty}^{\infty}dy'\int_{-\infty}^{\infty}dz'\frac{|\mathbf{f}_\pm(\theta',\phi')|^2}{|\mathbf{r}-\mathbf{r}'|^2}\ , \tag{3.17a}$$

where the x', y', and z' integrations can be easily evaluated, and the incoherent intensity is given by

$$I_i(\mathbf{r},\omega_\pm)=pL\frac{3\pi^2c}{16}\frac{|k_\pm|^6a^7e_\pm^2|\Gamma_\pm|^2}{|3\epsilon_h(\omega_\pm)+2\epsilon_b|^2}i_\pm(\theta_2)\ , \tag{3.17b}$$

where

$$i_\pm(\theta_2)=\cos^2\theta_2U_{21}^{\pm2}+\tfrac{8}{9}\sin^2\theta_2U_{20}^{\pm2}\ . \tag{3.17c}$$

IV. NUMERICAL RESULTS AND DISCUSSION

The microparticles to be considered in the numerical calculation are silver spheres with radius $a>20$ Å, where the quantum-size effect is not important.[10] The background dielectric constant ϵ_b and the plasma frequency ω_p of the silver spheres are, respectively, 5.578 and 3.8 eV. The damping constant ν inside the silver sphere is modified by the free-path effect[10] and is given by

$$\nu=\nu_B+\frac{v_F}{a}\ , \tag{4.1}$$

where $\nu_B=0.01\omega_P$ is the bulk damping constant and v_F is the Fermi velocity of the electrons.

For comparison, we plot the linear responses in Fig. 2 for a single silver sphere with $a=100$ Å in vacuum, which is irradiated by 0.3787-μm laser light of 1 MW intensity. The 0.3787-μm laser light can excite the surface dipole mode of the aforementioned silver sphere. Indeed, as shown in Fig. 2(b), the electric field inside the sphere is enhanced by the surface dipole resonant denominator $D(\omega_S)$, whose magnitude is about 10, and is nearly $\pi/2$ out of the phase with respect to the incident electric field. Figure 2(c) depicts the radial velocity throughout the microsphere.

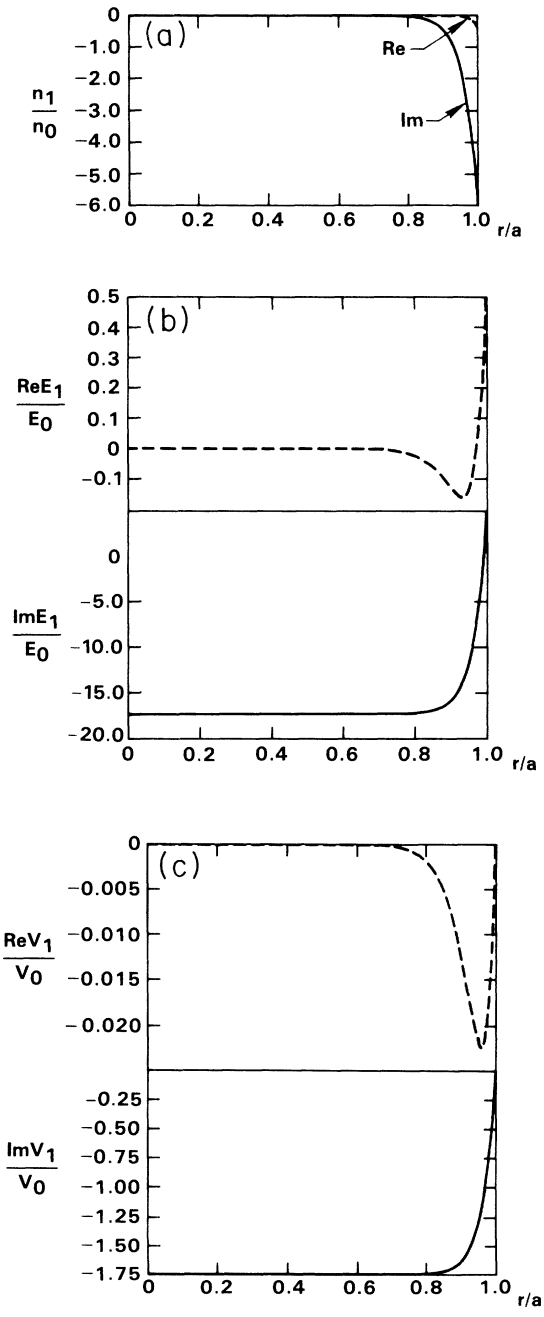

FIG. 2. Linear responses of a single silver sphere vs r/a, $a=100$ Å. The incident laser light is 1 MW at 0.3787 μm. The magnitude of incident electric field $E_0=0.92\times10^2$ statvolt/cm. (a) Electron density profile ($n_0=3.08\times10^{18}$ cm^{-3}), (b) radial electric field, and (c) radial velocity ($V_0=0.84\times10^5$ cm/sec).

In Figs. 3–5 are depicted the second-order responses with products of linear denominators of the aforementioned silver sphere for difference- and sum-frequency generation. To illustrate the surface-enhanced nature, the frequency of the first incident laser light is always tuned to the surface dipole resonant frequency, viz., $\omega_1=\omega_S$, in order to maximize the enhancement on the drive terms for the second-order fields. The frequency of the second laser light is tuned to the vicinity of ω_S, to optimize the second enhancement factor in the drive terms. Also, the second laser may be tuned to the frequency $\omega_2=\omega_S-\omega_q$. The intensity of both incident light beams are 1 MW/cm^2.

All the responses in Figs. 3–5 for the small difference frequency and the sum frequency at the surface quadrupole resonance are well screened, since the frequencies are below the plasma frequency. The responses in Figs. 3–5 for the sum-frequency generation near $2\omega_S$ are highly oscillatory.

For quadrupole ($l=2$) responses, the total charge is zero and the acoustic condition can be imposed as an additional boundary condition (ABC). However, for monopole ($l=0$) responses, one must ensure the charge conservation and the ABC is the charge neutrality instead of the acoustic condition. Thus the acoustic condition may be violated, which implies an electron flow across the

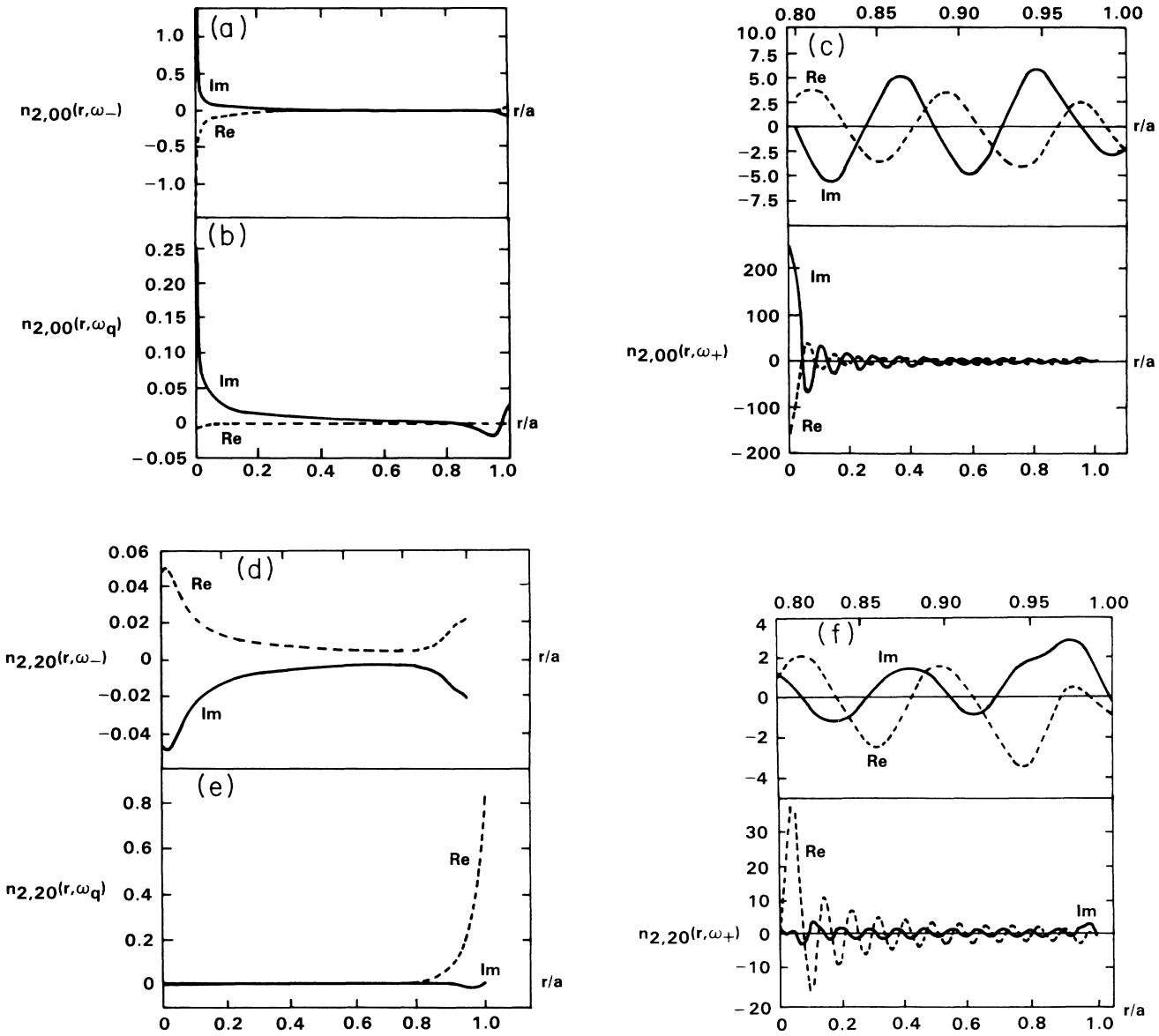

FIG. 3. Second-order dimensionless electron density profile $n_{2,lm}(r,\omega_\pm)$ vs r/a, $a=100$ Å. $\omega_1=\omega_S$, $l=0$, $m=0$, for (a), (b), and (c). $l=2$, $m=0$ for (d), (e), and (f). (a) and (d) for difference-frequency generation with $\omega_-=0.01\omega_p$, (b) and (e) for sum-frequency generation with $\omega_+=\omega_q=0.3642$ μm, and (c) and (f) for sum-frequency generation $\omega_\pm=2\omega_S-0.01\omega_p=0.1904$ μm. The units $\Gamma_\pm D(\omega_1)D(\omega_2)$ for $n_{2,lm}(r,\omega_\pm)$ are 1.89×10^{18} cm^{-3}.

boundary of the sphere.[8]

In Fig. 5, we observe that the acoustic condition is indeed violated for $l=0$. For the difference-frequency generation shown in Fig. 5(a), the radial velocity at the surface is nearly equal to the maximum velocity inside the sphere, where $v/\omega_- \sim 1$. For the sum-frequency generation near $2\omega_S$ shown in Fig. 5(c), the radial velocity at the surface is nearly zero, where $v/\omega_+ \sim 0.01$. Therefore, the ratio of the radial velocity at the surface to the maximum velocity inside the sphere is of the order of $v/\omega_\pm$ for $l=0$. Also, the $l=2$ second-order responses in Figs. 3(e), 4(e), and 5(e) are indeed enhanced with respect to the $l=0$ counterparts in Figs. 3(b), 4(b), and 5(b).

Finally, the coherent and incoherent intensities for a slab of tenuous silver microsphere composite embedded in a dispersive host will be calculated. The configuration is shown in Fig. 1. The dispersive host is chosen to be an artificial glass. The first incident frequency ω_1 is chosen to be the surface dipole frequency ω_S of a silver sphere in the glass host, viz., $\omega_1=\omega_S=0.4304$ μm, with $\epsilon_h(\omega_S)=2.15$. The second incident frequency ω_2 is either tuned to the vicinity of ω_S, viz., $\omega_2=\omega_S-0.05\omega_P=0.4608$, μm, with $\epsilon_h(\omega_2)=2.14$, or the frequency ω_2 may be the difference frequency between the surface dipole and quadrupole resonances, viz., $\omega_2=\omega_q-\omega_S$, with $\omega_q \simeq 0.4$ μm and $\epsilon_h(\omega_2)=1.9$.

The coherent intensity I_c of the sum- (ω_+) or difference- (ω_-) frequency generation peaks strongly near the perfect phase matching, viz., $\Delta_\pm L \leq 1$, where $\Delta_\pm$ is defined in Eq. (3.14) and L is the slab thickness. The phase mismatch $\Delta_\pm$ defines a coherent length $L_{\rm coh}=1/\Delta_\pm$. Only for $L<L_{\rm coh}$ is the coherent intensity significant, and it increases more or less quadratically with L. For a few-mm-thick silver microsphere composite, a sufficiently long coherent length $L_{\rm coh}$ is only achievable under the perfect phase matching, viz., $\Delta_\pm=0$.

In order to have perfect phase matching, we need the host dielectric constant ϵ_h at the sum (difference) frequency to be less (greater) than $\epsilon_h(\omega_1)$ and $\epsilon_h(\omega_2)$. The incident angle θ_2 is determined by $\epsilon_h(\omega_\pm)$ via the perfect phase-matching condition. The angle θ_2 will then set the coherent angle $\theta_\pm$ through the stationary condition given in Eq. (3.10c). It is no loss of generality to restrict the values of θ_2 to be in the range between 0° and 90°, since the range $90° \leq \theta_2 \leq 180°$ is just the mirror image of the former range with respect to the x-y plane. The physical

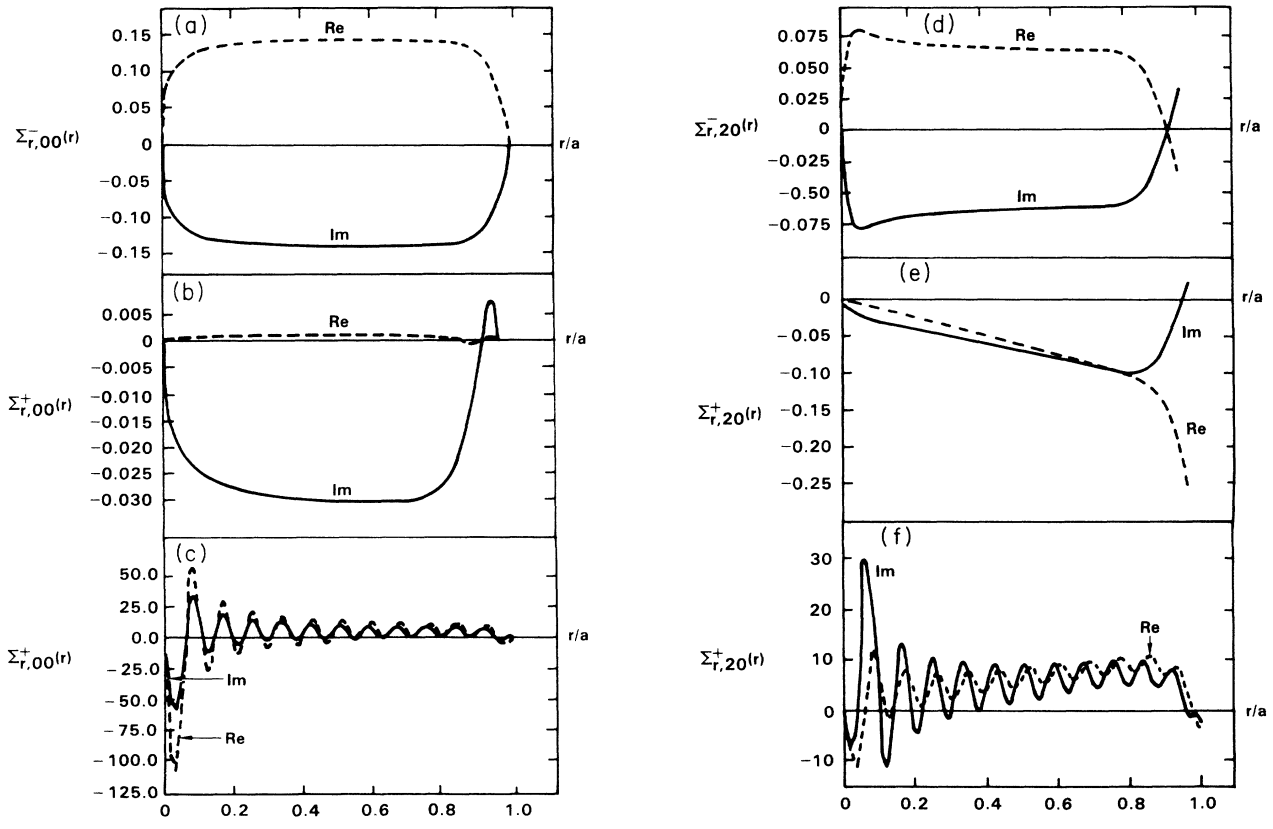

FIG. 4. Second-order dimensionless radial electric field $\Sigma^\pm_{r,lm}(r)$ vs r/a, $a=100$ Å. Same configuration treated in Fig. 2. $l=0$, $m=0$ for (a), (b), and (c). $l=2$, $m=0$ for (d), (e), and (f). (a) and (d) for $\omega_-=0.01\omega_p$, (b) and (e) for $\omega_+=\omega_q$, and (c) and (f) for $\omega_+=2\omega_S-0.01\omega_P$. The units $E_{20}D(\omega_1)D(\omega_2)$ for $\Sigma^\pm_{r,lm}(r)$ are 2.3 statvolt/cm.

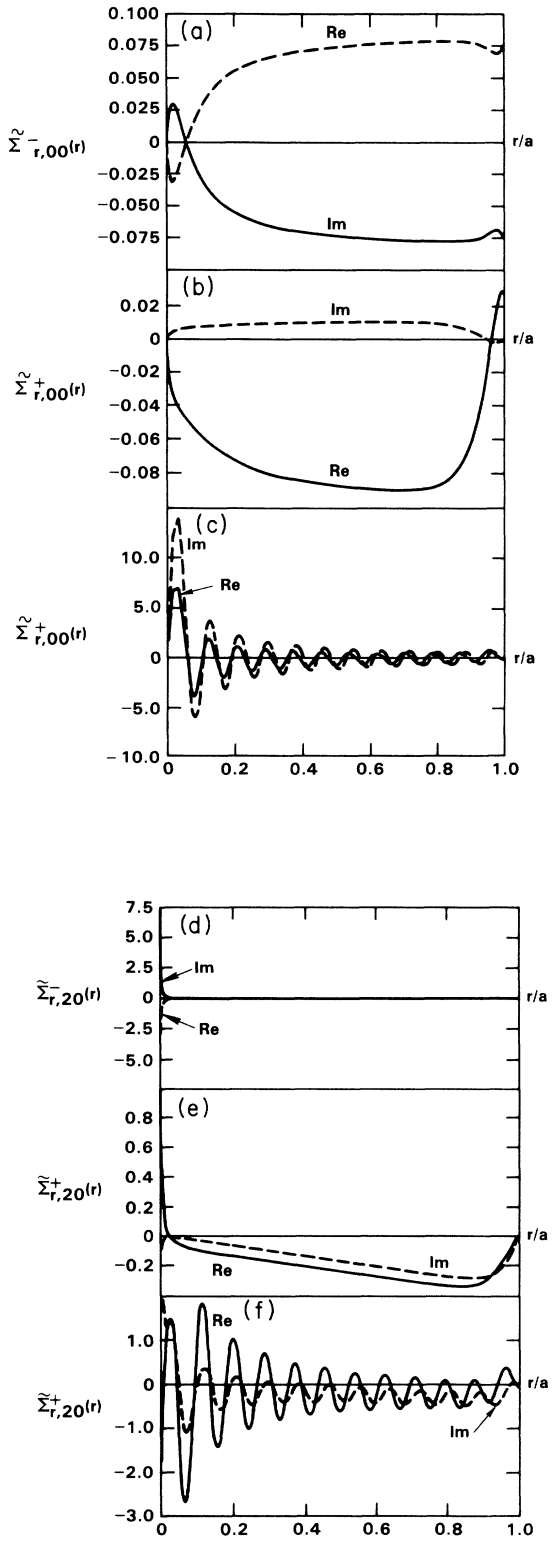

FIG. 5. Second-order dimensionless radial velocity $\tilde{\Sigma}^{\pm}_{r,lm}(r)$ vs r/a, $a=100$ Å. Same configuration treated in Fig. 2. $l=0$, $m=0$ for (a), (b), and (c). $l=2$, $m=0$ for (d), (e), and (f). (a) and (b) for $\omega_-=0.01\omega_P$ (unit $\bar{V}_{20}=6.4\times10^3$ cm/sec), (b) and (e) for $\omega_+=\omega_q$ (unit $\bar{V}_{20}=3.5\times10^3$ cm/sec), and (c) and (f) for $\omega_+=2\omega_S-0.01\omega_P$ (unit $\bar{V}_{20}=1.7\times10^4$ cm/sec). $\bar{V}_{20}=V_{20}D(\omega_1)D(\omega_2)$.

values of θ_2 are going to limit the possible choices of the host materials, viz., $\epsilon_h(\omega_\pm)$. A slab of silver microsphere composite to be considered consists of radius $a=100$ Å, thickness $L=1$ mm, and volume fraction $p=10^{-4}$. Figure 6 shows the dependence of the incident and coherent angles on $\epsilon_h(\omega_\pm)$. For the sum-frequency generation near $2\omega_S$ or at ω_q, the possible choices of $\epsilon_h(\omega_\pm)$ are, respectively, in the range of (1.08,2.14) or (1.8,2.13). The difference-frequency generation at $\omega_-=0.05\omega_p$ requires that $2.3\le\epsilon_h(\omega_-)<900$.

Figure 7 shows the dependence of the coherent and incoherent intensities upon $\epsilon_h(\omega_\pm)$. The reduced coherent and incoherent intensities are $i_c^{\pm}(\theta_2)/|U_{20}^{\pm}|^2$ and $i^{\pm}(\theta_2)/|U_{20}^{\pm}|^2$, respectively. The conversion factor to the corresponding absolute intensity is given in the figure caption for each case. The coherent intensity of the sum-frequency generation near $2\omega_S$ is about 1 W/cm^2,

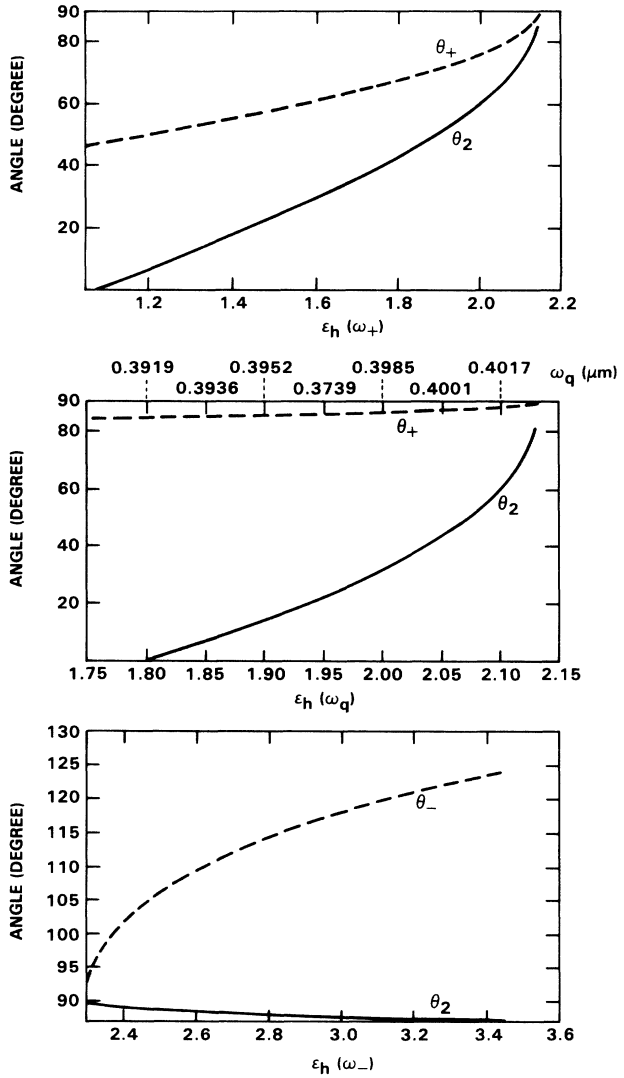

FIG. 6. Incident θ_2 and coherent $\theta_\pm$ angles vs $\epsilon_h(\omega_\pm)$. (a) $\omega_+=2\omega_S-0.05\omega_p=0.2225$ μm, (b) $\omega_q=0.39$–0.41 μm, and (c) $\omega_-=0.05\omega_P=6.54$ μm. $p=10^{-4}$, $L=1$ mm, and $a=100$ Å.

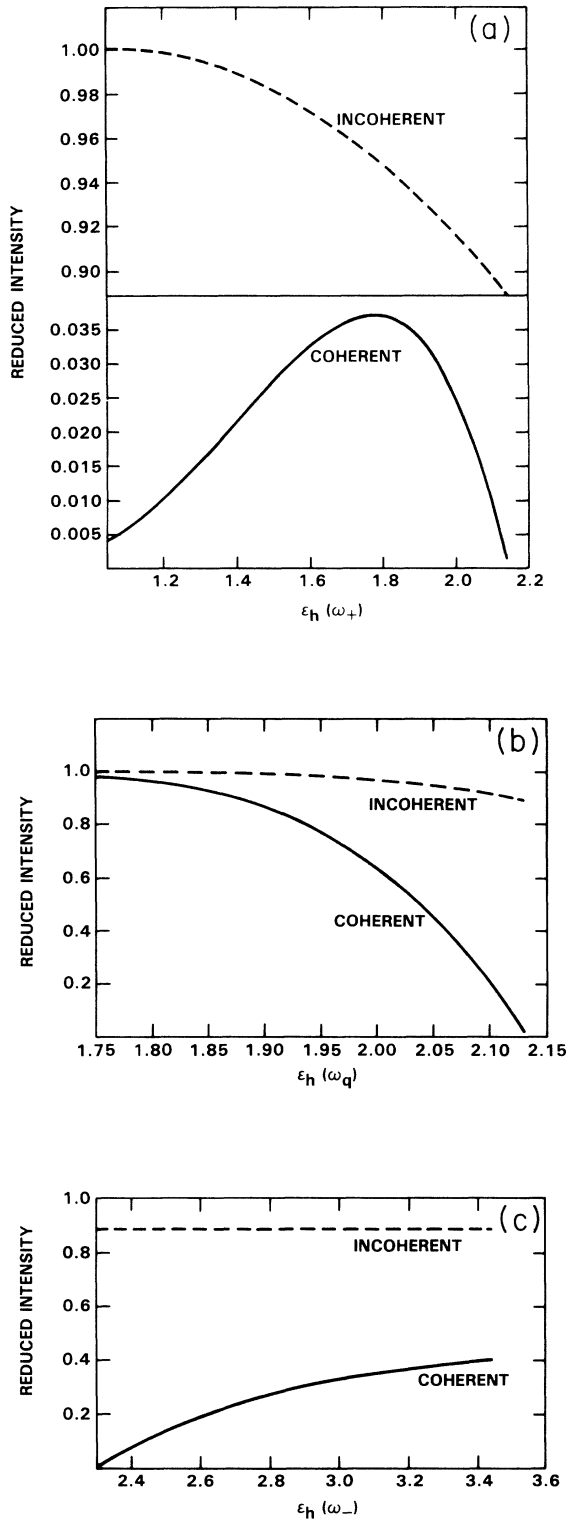

FIG. 7. Reduced coherent and incoherent intensities vs $\epsilon_h(\omega_\pm)$. (a) $\omega_+=2\omega_S-0.05\omega_P$. The conversion factors are 29.19 and 0.12 W/cm^2 for coherent and incoherent intensities. (b) $\omega_+=\omega_q$, the conversion factors are 0.23 W/cm^2 and 0.30 mW/cm^2 for coherent and incoherent intensities. (c) $\omega_-=0.05\omega_q$, the conversion factors are 13.76 μW/cm^2 and 6.65 nW/cm^2 for the coherent and incoherent intensity. $p=10^{-4}$, $L=1$ mm, and $a=100$ Å.

which is 10 dB above the corresponding incoherent intensity for $1.2\leq\epsilon_h(\omega_\pm)\leq 2.1$. The coherent intensity of the sum-frequency generation at ω_q is 0.05–0.2 W/cm^2, which is 27–30 dB above the incoherent intensity for $1.75\leq\epsilon_h(\omega_q)\leq 2.1$. The coherent intensity at the difference frequency at $\omega_-=0.05\omega_p$ is only 1–10 μW/cm^2, which is 40–50 dB above the incoherent counterpart for $\epsilon_h(\omega_-)\geq 2.4$. For the sum-frequency generation, the incoherent intensity may still be detectable. However, for the difference-frequency generation, only the coherent intensity can be observed with ease.

APPENDIX A

To solve Eq. (2.7a) for a sphere, we expand the electron density in the following series:

$$n_1(\mathbf{r},\omega_j)=\sum_{l,m} A_{lm}(q_j a)i_l(q_j r)Y_{lm}(\theta,\phi)\ , \tag{A1}$$

where a is the radius of the sphere, $i_n(z)$ is the nth-order modified spherical Bessel function of $q_j=q(\omega_j)$, in spherical coordinate $\mathbf{r}=(r,\theta,\phi)$, and $Y_{lm}(\theta,\phi)$ is the spherical harmonic of order (l,m). Since the ω_1 laser beam is linearly polarized in the z direction, $n_1(\mathbf{r},\omega_1)$ consists only of the $l=1$, $m=0$ term. The ω_2 laser beam is linearly polarized in the $\hat{\mathbf{e}}_2=(\hat{\mathbf{x}}\cos\theta_2+\hat{\mathbf{z}}\sin\theta_2)$ direction, and $n_1(\mathbf{r},\omega_2)$ contains the $l=1$, $m=\pm 1$ term (see Fig. 1). Applying the boundary conditions at the surface yields the following solutions for the first-order electron density at the two laser frequencies:

$$n_1(\mathbf{r},\omega_1)=\frac{\epsilon_b}{4\pi e a}N(r,\omega_1)A_1\cos\theta/D_1(\omega_1)\ , \tag{A2a}$$

$$n_1(\mathbf{r},\omega_2)=\frac{\epsilon_b}{4\pi e a}N(r,\omega_2)A_2(\sin\theta_2\cos\theta + \cos\theta_2\sin\theta\cos\phi)/D_1(\omega_2)\ . \tag{A2b}$$

The boundary conditions yield the following expression for $N(r,\omega_j)$:

$$N(r,\omega_j)=3\epsilon_h(\omega_j)q_j a i_1(q_j r)/\Omega_j i_1'(q_j a)\ , \tag{A2c}$$

where $i_1'(z)$ implies the derivative with respect to z, and the denominator $D_1(\omega_j)$ is given by

$$D_1(\omega_j)=\epsilon_b(1-1/\Omega_j) + 2\epsilon_h(\omega_j)[1-i_1(q_j a)/\Omega_j q_j a i_1'(q_j a)]\ , \tag{A2d}$$

with $\Omega_j\equiv\omega_j(\omega_j+i\nu)/\omega_p^2$ and ν is assumed to be frequency independent. The real part of this important denominator vanishes at ω_S. This denominator dominates the electrodynamics of microparticle composites, whenever the surface (or Frohlich) dipole mode is excited by $\omega_j=\omega_S$.

The first-order electric field $\mathbf{E}_1(\mathbf{r},\omega_j)$ is given by

$$E_{1r}(\mathbf{r},\omega_1)=\Sigma_r(r,\omega_1)A_1\cos\theta/D_1(\omega_1)\ , \tag{A3a}$$

$$E_{1r}(\mathbf{r},\omega_2)=\Sigma_r(r,\omega_2)A_2(\sin\theta_2\cos\theta + \cos\theta_2\sin\theta\cos\phi)/D_1(\omega_2) \tag{A3b}$$

$$E_{1\theta}(\mathbf{r},\omega_1)=-\Sigma_\theta(r,\omega_1)A_1\sin\theta/D_1(\omega_1)\ , \tag{A3c}$$

$$E_{1\theta}(\mathbf{r},\omega_2)=\Sigma_\theta(r,\omega_2)A_2(\cos\theta_2\cos\theta\cos\phi - \sin\theta_2\sin\theta)/D_1(\omega_2)\ , \tag{A3d}$$

$$E_{1\phi}(\mathbf{r},\omega_1)=0\ , \tag{A3e}$$

$$E_{1\phi}(\mathbf{r},\omega_2)=-\Sigma_\theta(r,\omega_2)A_2\cos\theta_2\sin\phi\ , \tag{A3f}$$

where

$$\Sigma_r(r,\omega_j)=3\epsilon_h(\omega_j)[1-i_1'(q_jr)/\Omega_j i_1'(q_ja)]\ , \tag{A3g}$$

$$\Sigma_\theta(r,\omega_j)=3\epsilon_h(\omega_j)[1-i_1(q_jr)/\Omega_j q_j r i_1'(q_ja)]\ . \tag{A3h}$$

The first-order electron drift velocity $\mathbf{v}_1(\mathbf{r},\omega_j)$ is

$$v_{1r}(\mathbf{r},\omega_1)=\tilde{\Sigma}_r(r,\omega_1)v_{10}\cos\theta/D_1(\omega_1)\ , \tag{A4a}$$

$$v_{1r}(\mathbf{r},\omega_2)=\tilde{\Sigma}_r(r,\omega_2)v_{20}(\sin\theta_2\cos\theta + \cos\theta_2\sin\theta\cos\phi)/D_1(\omega_2)\ , \tag{A4b}$$

$$v_{1\theta}(\mathbf{r},\omega_1)=-\tilde{\Sigma}_\theta(r,\omega_1)v_{10}\sin\theta/D_1(\omega_1)\ , \tag{A4c}$$

$$v_{1\theta}(\mathbf{r},\omega_2)=\tilde{\Sigma}_\theta(r,\omega_2)v_{20}(\cos\theta_2\cos\theta\cos\phi - \sin\theta_2\sin\theta)/D_1(\omega_2)\ , \tag{A4d}$$

$$v_{1\phi}(\mathbf{r},\omega_1)=0\ , \tag{A4e}$$

$$v_{1\phi}(\mathbf{r},\omega_2)=-\tilde{\Sigma}_\theta(r,\omega_2)v_{20}\cos\theta_2\sin\phi/D_1(\omega_2)\ , \tag{A4f}$$

where $v_{j0}=-ieA_j/m(\omega_j+i\nu)$ and the various $\tilde{\Sigma}_\mu$ are defined as

$$\tilde{\Sigma}_r(r,\omega_j)=3\epsilon_h(\omega_j)[1-i_1'(q_jr)/i_1'(q_ja)]\ , \tag{A4g}$$

$$\tilde{\Sigma}_\theta(r,\omega_j)=3\epsilon_h(\omega_j)[1-i_1(q_jr)/i_1'(q_ja)q_jr]\ . \tag{A4h}$$

APPENDIX B

First, the different components $S^{\pm}_{\mu_{lm}}(r')$ of the driver term $\mathbf{S}^{\pm}(\mathbf{r})$ in Eqs. (2.11) depend only weakly on frequency and do not reflect the surface-mode resonances of the microparticles, and are defined below:

$$S^{\pm}_{r_{00}}(r)=S^{\pm}_{r_{20}}(r)-3[\tilde{\Sigma}_\theta(r,\omega_1)\tilde{\Sigma}_r(r,\pm\omega_2)+\tilde{\Sigma}_\theta(r,\pm\omega_2)\tilde{\Sigma}_r(r,\omega_1)]L^{\pm}a/r\ , \tag{B1a}$$

$$\begin{aligned}S^{\pm}_{r_{20}}(r)=&N_1(r,\omega_1)\Sigma_r(r,\pm\omega_2)+N_2(r,\pm\omega_2)\Sigma_r(r,\omega_1)\\&+N_1(r,\omega_1)\tilde{\Sigma}_r(r,\pm\omega_2)\omega_1/(\pm\omega_2+i\nu)\pm N_1(r,\pm\omega_2)\tilde{\Sigma}_r(r,\omega_1)\omega_2/(\omega_1+i\nu)\\&-L^{\pm}[\tilde{\Sigma}_r(r,\omega_1)\tilde{\Sigma}_r'(r,\pm\omega_2)-\tilde{\Sigma}_\theta(r,\omega_1)\tilde{\Sigma}_r(r,\pm\omega_2)a/r]-L^{\pm}[\tilde{\Sigma}_r(r,\pm\omega_2)\tilde{\Sigma}'(r,\omega_1)-\tilde{\Sigma}_\theta(r,\pm\omega_2)\tilde{\Sigma}_r(r,\omega_1)a/r]\\&+\tfrac{2}{3}(\beta/\omega_pa)^2[N_1(r,\omega_1)N_1'(r,\pm\omega_2)+N_1(r,\pm\omega_2)N_1'(r,\omega_1)]\ ,\end{aligned} \tag{B1b}$$

$$S^{\pm}_{\theta_{20}}(r)=S_{\theta C}(r,\omega_1,\pm\omega_2)+S_{\theta S}(r,\omega_1,\pm\omega_2)\ , \tag{B1c}$$

$$S^{\pm}_{\phi_{21}}(r)=S_\phi(r,\omega_1,\pm\omega_2)+S_\phi(r,\pm\omega_2,\omega_1)\ , \tag{B1d}$$

and

$$S_{\theta C}(r,\omega_1,\pm\omega_2)=S_\phi(r,\omega_1,\pm\omega_2)+\tilde{\Sigma}_\theta(r,\pm\omega_2)\tilde{\Sigma}_\theta(r,\omega_1)L^{\pm}a/r\ , \tag{B1e}$$

$$S_{\theta S}(r,\omega_1,\pm\omega_2)=S_{\theta C}(r,\pm\omega_2,\omega_1)\ , \tag{B1f}$$

$$\begin{aligned}S_\phi(r,\omega_1,\pm\omega_2)=&N_1(r,\omega_1)\Sigma_\theta(r,\pm\omega_2)+N_1(r,\omega_1)\tilde{\Sigma}_\theta(r,\pm\omega_2)\omega_1/(\pm\omega_2+i\nu)\\&-\tilde{\Sigma}_r(r,\omega_1)\tilde{\Sigma}_\theta'(r,\pm\omega_2)L^{\pm}+\tfrac{2}{3}(\beta/\omega_pa)^2N_1(r,\omega_1)N_2(r,\pm\omega_2)a/r\ ,\end{aligned} \tag{B1g}$$

where the dimensionless linear electron density $N_1(r,\omega_j)$ is given in Eq. (A2c) and the $L^{\pm}$ function is defined by

$$L^{\pm}=\omega_p^2[(\omega_1+i\nu)(\pm\omega_2+i\nu)]^{-1}\ , \tag{B2a}$$

and the primed functions are defined as

$$F'(r,\omega_j)=a\frac{\partial F(r,\omega_j)}{\partial r}\ . \tag{B2b}$$

Then, to solve Eqs. (2.8) for a sphere, we again expand $n_2(\mathbf{r},\omega_\pm)$ in terms of spherical harmonics as $n_1(\mathbf{r},\omega_j)$:

$$n_2(\mathbf{r},\omega_\pm)=\sum_{l,m}B_{lm}(q_\pm a)i_l(q_\pm r)Y_{lm}(\theta,\phi) + \int d\mathbf{r}'[\mathbf{G}_S(q_\pm|\mathbf{r},\mathbf{r}')\nabla\cdot\mathbf{S}_\pm(\mathbf{r}')]/\beta^2\ , \tag{B3a}$$

where the integral is an inhomogeneous term and the coefficients B_{lm} are determined by the boundary conditions. The Green's function $\mathbf{G}_S(q_\pm|\mathbf{r},\mathbf{r}')$ is given by

$$\mathbf{G}_S(q_\pm|\mathbf{r},\mathbf{r}')=q_\pm\sum_l i_l(q_\pm r_<)k_l(q_\pm r_>) \times Y^*_{lm}(\theta',\phi')Y_{lm}(\theta,\phi)\ , \tag{B3b}$$

where the asterisk implies complex conjugate. The sum- and difference-frequency fields obey the Laplace equation

$$\nabla^2\Phi_2(\mathbf{r},\omega_\pm)=0 \tag{B4a}$$

outside the microparticle, and the Poisson equation

$$\nabla^2\Phi_2(\mathbf{r},\omega_\pm)=4\pi e n_2(\mathbf{r},\omega_\pm)/\epsilon_b \tag{B4b}$$

within it. Equation (B4) will be solved by expanding in spherical harmonics. Thus, outside the sphere, we have

$$\Phi_2(\mathbf{r},\omega_\pm)=\sum_{l,m} C_{lm}(q_\pm a)r^{-(l+1)}Y_{lm}(\theta,\phi)\ . \tag{B5a}$$

The electrostatic potential inside the microparticle is driven by the second-order charge density $n_2(\mathbf{r},\omega_\pm)$. Thus, within this region, we write the second-order electrostatic potential as

$$\Phi_2(\mathbf{r},\omega_\pm)=\sum_{l,m} D_{lm}(q_\pm a)r^l Y_{lm}(\theta,\phi) -(4\pi e/\epsilon_b)\int d\mathbf{r}'\,\mathbf{G}_0(\mathbf{r},\mathbf{r}')n_2(\mathbf{r}',\omega_\pm)\ , \tag{B5b}$$

where $\mathbf{G}_0(\mathbf{r},\mathbf{r}')$ is the Green's function for the Laplace equation. The coefficients for the various multiple fields, C_{lm} and D_{lm}, are determined by the electrostatic boundary conditions at the surface of the microsphere. The first-order fields exhibit a dipolar character outside the microparticle, viz., the electrostatic fields consist of $l=1$, $m=0$ at ω_1, and $l=1$ $m=\pm1$ at ω_2. Thus the second-order fields should have monopole and quadrupole characters. The second-order electrostatic field should consist of $l=0$ and the $l=2$, $m=(0,\pm1)$ terms. However, a monopole field vanishes by change conservation. Hence only the coefficients for the quadrupole contribute, i.e., $D_{20}(C_{20})$ and $D_{2\pm1}(C_{2\pm1})$ are nonzero. Finally, the second-order drift velocity $\mathbf{v}_2(\mathbf{r},\omega_\pm)$ can be expressed in terms of $n_2(\mathbf{r},\omega_\pm)$ and $\Phi_2(\mathbf{r},\omega_\pm)$ via Euler's equation and given by

$$\mathbf{v}_2(\mathbf{r},\omega_\pm)=\mathbf{v}_2''(\mathbf{r},\omega_\pm)+\mathbf{v}_2'(\mathbf{r},\omega_\pm)\ , \tag{B6a}$$

where

$$\mathbf{v}_2''(\mathbf{r},\omega_\pm)=-i[\mathbf{S}_\pm(\mathbf{r})-(n_0e/m)\nabla\Phi_2(\mathbf{r},\omega_\pm) +\beta^2\nabla n_2(\mathbf{r},\omega_\pm)]/n_0(\omega_\pm+i\nu)\ , \tag{B6b}$$

and

$$\mathbf{v}_2'(\mathbf{r},\omega_\pm)=-\frac{1}{n_0}n_1(\mathbf{r},\omega_1)\mathbf{v}_1(\mathbf{r},\pm\omega_2) -\frac{1}{n_0}n_1(\mathbf{r},\pm\omega_2)\mathbf{v}_1(\mathbf{r},\omega_1)\ . \tag{B6c}$$

Equations (B1)–(B5), along with the boundary conditions on the drift velocity and the electrostatic potential, completely determine the unknown coefficients B_{lm}, C_{lm}, and D_{lm}. It is a tedious, but a straightforward task to obtain the following expression for the density $n_2(\mathbf{r},\omega_\pm)$:

$$n_2(\mathbf{r},\omega_\pm)=\Gamma_\pm\{(4\pi/9)^{1/2}n_{2,00}(r,\omega_\pm)\sin\theta_2 Y_{00}(\theta)+(16\pi/45)^{1/2}n_{2,20}(r,\omega_\pm)\sin\theta_2 Y_{20}(\theta) +(2\pi/15)^{1/2}n_{2,21}(r,\omega_\pm)\cos\theta_2[Y_{21}(\theta,\phi)-Y_{2-1}(\theta,\phi)]\}\ , \tag{B7a}$$

where

$$\Gamma_\pm\equiv\epsilon_b A_1 A_2 q_\pm a/4\pi m\beta^2 D(\omega_1)D(\omega_2)\ , \tag{B7b}$$

where $q_\pm=[\omega_p^2-\omega_\pm(\omega_\pm+i\nu)]^{1/2}/\beta$. The quantity $\Gamma_\pm$, which has units of density, exhibits resonant behavior if ω_1 and/or ω_2 lie near the surface dipole mode frequency ω_s. This feature of the second-order density response follows directly from the drive term $\mathbf{S}_\pm(\mathbf{r})$. An examination of Eq. (B7a) reveals the important role of the initial geometry as manifested in the angle θ_2. If the two laser beams are collinear $\theta_2=\pi/2$, then the system retains cylindrical symmetry and the electron density is independent of ϕ. On the other hand, if the incident laser beams are orthogonal $\theta_2=0$, then the $l=2$, $m=0$ terms vanish.

The dimensionless functions in monopole and quadrupole radial density $n_{2,00}(r,\omega_\pm)$ and $n_{2,2m}(r,\omega_\pm)$ are given by

$$n_{2,00}(r,\omega_\pm)=i_0(q_\pm r)J_{00S}(a,\omega_\pm)/i_1(q_\pm a)-J_{00}(r,\omega_\pm)\ , \tag{B7c}$$

$$n_{2,2m}(r,\omega_\pm)=\bar{J}_{2m}(a,\omega_\pm)i_2(q_\pm r)/D_2(\omega_\pm)-J_{2m}(r,\omega_\pm)\ , \tag{B7d}$$

where the denominator $D_2(\omega_\pm)$, which appears only in the quadrupole radial density terms in Eq. (B7d), is given by

$$D_2(\omega_\pm)=2\epsilon_b\left[1-\frac{1}{\Omega_\pm}\right] +3\epsilon_h(\omega_\pm)[1-2i_2(q_\pm a)/\Omega_\pm q_\pm a i_2'(q_\pm a)]\ , \tag{B8}$$

where $\Omega_\pm=\omega_\pm(\omega_\pm+i\nu)/\omega_p^2$. Note that $D_2(\omega_\pm)$ is a function only of $\omega_\pm$, not ω_1 or ω_2 individually. This feature follows from the fact that $D_2(\omega_\pm)$ reflects the possibility of exciting a surface mode if $\omega_\pm$ coincides with a quadrupole Fröhlich surface resonant frequency ω_q.

In Eqs. (B7), the functions $J_{lm}(r,\omega_\pm)$ are defined as

$$J_{lm}(r,\omega_\pm)=k_l(q_\pm r)j_{lm}^<(r,\omega_\pm)+i_l(q_\pm r)j_{lm}^>(r,\omega_\pm)\ , \tag{B9a}$$

where $(l,m)=(0,0)$, (2,0), and (2,1), and two functions J_{00S} and $\bar{J}_{2m}$ are defined by

$$J_{00S}(r,\omega_\pm)=\frac{q_\pm}{a^2}\int_0^r dr' r'^2 J_{00}(r',\omega_\pm)\ , \tag{B9b}$$

$$\bar{J}_{2m}(r,\omega_\pm)=[3\epsilon_h(\omega_\pm)+2\epsilon_b]\times\left[1-\frac{1}{\Omega_\pm}\right]J'_{2m}(a,\omega_\pm)/i'_2(q_\pm a)+3\epsilon_h(\omega_\pm)J_{2mS}(a,\omega_\pm)/\Omega_\pm i'_2(q_\pm a)\ , \quad \text{(B9c)}$$

with

$$J'_{lm}(r,\omega_\pm)=k'_l(q_\pm r)j^<_{lm}(r,\omega_\pm)+i'_l(q_\pm r)j^>_{lm}(r,\omega_\pm)\ , \quad \text{(B9d)}$$

$$J_{2mS}(r,\omega_\pm)=\frac{q_+}{a^4}\int_0^r dr' r'^4 J_{2m}(r',\omega_\pm)\ . \quad \text{(B9e)}$$

The functions $j^<_{lm}(r,\omega_\pm)$ and $j^>_{lm}(r,\omega_\pm)$ are given by

$$j^<_{00}(r,\omega_\pm)=(q_\pm/a^2)\int_0^r dr' r'^2 i'_0(q_\pm r')S_{r_{00}}(r')\ , \quad \text{(B10a)}$$

$$j^>_{00}(r,\omega_\pm)=(q_\pm/a^2)\int_r^a dr' r'^2 k'_0(q_\pm r')S^\pm_{r_{00}}(r')\ , \quad \text{(B10b)}$$

$$j^<_{2m}(r,\omega_\pm)=(q_\pm/a^2)\int_0^r dr' r'^2 i'_2(q_\pm r')S^\pm_{r_{20}}(r')+(3/a^2)\int_0^r dr' r' i_2(q_\pm r')S^\pm_{\theta_{2m}}(r')\ , \quad \text{(B10c)}$$

and

$$j^>_{2m}(r,\omega_\pm)=(q_\pm/a^2)\int_r^a dr' r'^2 k_2(q_\pm r')S^\pm_{r_{20}}(r')+(3/a^2)\int_r^a dr'\, r' k_2(q_\pm r')S^\pm_{\theta_{2m}}(r')\ , \quad \text{(B10d)}$$

where

$$S^\pm_{\theta_{21}}(r)=\tfrac{1}{6}S_{\theta C}(r,\omega_1,\pm\omega_2)+S_{\theta S}(r,\omega_1,\pm\omega_2)+\tfrac{5}{6}S^\pm_{\phi_{21}}(r)\ , \quad \text{(B10e)}$$

and the rest of $S^\pm_{\mu_{lm}}(r)$ are given in Eqs. (B1).

Next, we focus on the electric component of the second-order electric fields oscillating at the sum and difference frequencies in the vicinity of the microparticle. Inside the particle, the various components of the electric field are given by

$$E_{2r}(\mathbf{r},\omega_\pm)=E_{20}\{(4\pi/9)^{1/2}\sin\theta_2 Y_{00}(\theta)\Sigma^\pm_{r,00}(r)+(16\pi/45)^{1/2}\sin\theta_2 Y_{20}(\theta)\Sigma^\pm_{r,20}(r)-(2\pi/15)^{1/2}\cos\theta_2\times[Y_{21}(\theta,\phi)-Y_{2-1}(\theta,\phi)]\Sigma^\pm_{r,21}(r)\}\ , \quad \text{(B11a)}$$

$$E_{2\theta}(\mathbf{r},\omega_\pm)=E_{20}[-\sin\theta_2\sin2\theta\Sigma^\pm_{\theta,20}(r)+\cos\theta_2\cos2\theta\cos\phi\Sigma^\pm_{\theta,21}(r)]\ , \quad \text{(B11b)}$$

$$E_{2\phi}(\mathbf{r},\omega_\pm)=-E_{20}\cos\theta_2\cos\theta\sin\phi\Sigma^\pm_{\theta,21}(r)\ , \quad \text{(B11c)}$$

where

$$E_{20}=4\pi e\Gamma_\pm/\epsilon_b q_\pm\ . \quad \text{(B12)}$$

Thus the second-order electric fields have r, θ, and ϕ components. This complex polarization structure arises from the fact that the incident fields for the noncollinear configuration break the cylindrical symmetry of the system, a point which is underscored by the fact that the ϕ component of the electric field vanishes; viz., the cylindrical symmetry is restored, if the two laser beams are collinear (i.e., $\theta_2=\pi/2$). The functions $\Sigma^\pm_{a,lm}(r)$ are dimensionless field strengths which are defined by

$$\Sigma^\pm_{r,00}(r)=(a/r)^2 J_{00S}(r,\omega_\pm)-J_{00S}(a,\omega_\pm)i_1(q_\pm r)/i_1(q_\pm a)\ , \quad \text{(B13a)}$$

$$\Sigma^\pm_{r,2m}(r)=2Q_\pm\Sigma_{2m}(a,\omega_\pm)r/a+\Sigma_{2m}(r,\omega_\pm)-\tfrac{2}{3}\Sigma_{2mG}(r,\omega_\pm)\ , \quad \text{(B13b)}$$

$$\Sigma_{\theta,2m}(r,\omega_\pm)=Q_\pm\Sigma_{2m}(a,\omega_\pm)r/a-[\Sigma_{2m}(r,\omega_\pm)+\Sigma_{2mG}(r,\omega_\pm)]/3\ , \quad \text{(B13c)}$$

where $Q_\pm=[\epsilon_h(\omega_\pm)-\epsilon_b]/[3\epsilon_h(\omega_\pm)+2\epsilon_b]$. The functions $\Sigma_{2m}(r,\omega_\pm)$ and $\Sigma_{2mG}(r,\omega_\pm)$ are defined as

$$\Sigma_{2m}(r,\omega_\pm)=\tfrac{3}{5}[(a/r)^4 J_{2mS}(r,\omega_\pm)-\bar{J}_{2m}(r,\omega_\pm)i_3(q_\pm r)/D_2(\omega_\pm)]\ , \quad \text{(B14a)}$$

$$\Sigma_{2mG}(r,\omega_\pm)=\tfrac{3}{5}\{q_\pm r J_{2mG}(r,\omega_\pm)-\bar{J}_{2m}(r,\omega_\pm)[i_1(q_\pm r)-i_1(q_\pm a)r/a]/D_2(\omega_\pm)\}\ , \quad \text{(B14b)}$$

with J_{00S}, $\bar{J}_{2mS}$, and J_{2mS} given in Eqs. (B9b), (B9c), and (B9e), and

$$J_{2mG}(r,\omega_\pm)=\int_r^a dr' J_{2m}(r',\omega_\pm)/r'\ . \quad \text{(B15)}$$

The electric field inside the microparticle has two possible frequencies where a surface-mode resonance can be excited. Specifically, the presence of the $\Gamma_\pm$ factor implies possible resonant enhancement of the field if ω_1 and/or ω_2 coincide with the surface dipolar mode. Further, the $D_2(\omega_\pm)$ resonant denominator in Eqs. (B14) implies that the quadrupole surface mode at $\omega_\pm$ can also amplify the field. In actual practice, it is not possible to have all three frequencies ω_1, ω_2, and $\omega_\pm$ coincide with a Fröhlich resonance for the second-order processes discussed here.

Outside the microparticle, the electric fields are quadrupolar in nature. In the near (static) zone, the electrostatic potential of a sphere is given by

$$\Phi_2(\mathbf{r},\omega_\pm)=\tfrac{1}{3}\{(16\pi/45)^{1/2}Y_{20}(\theta)Q_{zz} -(2\pi/15)^{1/2}[Y_{21}(\theta,\phi) -Y_{2-1}(\theta,\phi)]Q_{xz}\}/r^3 . \tag{B16}$$

The components of the quadrupole moment $Q_{\mu\nu}$ in terms of the dimensionless quantities U_{2j} are given by

$$Q_{zz}=-16\pi e\Gamma_\pm\sin\theta_2 U^\pm_{20}a^5/3[3\epsilon_h(\omega_\pm)+2\epsilon_b] , \tag{B17a}$$

$$Q_{xz}=-4\pi e\Gamma_\pm\cos\theta_2 U^\pm_{21}a^5/[3\epsilon_h(\omega_\pm)+2\epsilon_b] , \tag{B17b}$$

where $U^\pm_{2m}$ is the dimensionless function in the quadrupole moments and given by

$$U^\pm_{2m}=\frac{1}{a^5}\int_0^a r^4\,dr\,n_{2,2m}(r,\omega_\pm) \tag{B18a}$$

$$=[\bar{J}_{2m}(a,\omega_\pm)i_3(q_\pm a)/D_2(\omega_\pm) -J_{2mS}(a,\omega_\pm)]/q_\pm a . \tag{B18b}$$

As expected, the quadrupole moments and the electrostatic field outside the microparticle are also surface enhanced if either of the frequencies ω_1 or ω_2 coincides with the surface dipole resonance (from $I_\pm$) or $\omega_\pm$ with the surface quadrupole resonance from $D_2(\omega_\pm)$.

The second-order electron drift velocity $\mathbf{v}''_2(\mathbf{r},\omega_\pm)$ in Eq. (B6a) is given by

$$v''_{2r}(\mathbf{r},\omega_\pm)=V_{20}\{(4\pi/9)^{1/2}\sin\theta_2 Y_{00}(\theta)\tilde{\Sigma}^\pm_{r,00}(r)+(16\pi/45)^{1/2}\sin\theta_2 Y_{20}(\theta)\tilde{\Sigma}^\pm_{r,20}(r) -(2\pi/15)^{1/2}\cos\theta_2[Y_{21}(\theta,\phi)-Y_{2-1}(\theta,\phi)]\tilde{\Sigma}^\pm_{\theta,21}(r)\} , \tag{B19a}$$

$$v''_{2\theta}(\mathbf{r},\omega_\pm)=V_{20}[-\sin\theta_2\sin2\theta\tilde{\Sigma}^\pm_{\theta,20}(r)+\cos\theta_2\cos2\theta\cos\phi\tilde{\Sigma}^\pm_{\theta,21}(r)] , \tag{B19b}$$

$$v''_{2\phi}(r,\omega_\pm)=-V_{20}\cos\theta_2\cos\theta\sin\phi\tilde{\Sigma}^\pm_{\phi,21}(r) , \tag{B19c}$$

where

$$V_{20}=-i\beta^2 q_\pm\Gamma_\pm/n_0(\omega_\pm+i\nu) , \tag{B20}$$

and the dimensionless functions $\tilde{\Sigma}^\pm_{a,lm}(r)$ are given by

$$\tilde{\Sigma}_{r,00}(r)=J_{00S}(a,\omega_\pm)i_1(q_\pm r)/i_1(q_\pm a) -J'_{00}(r,\omega_\pm)+\Sigma_{r,00}(r)q^2_{\rm TF}/q^2_\pm , \tag{B21a}$$

$$\tilde{\Sigma}^\pm_{r,2m}(r)=\bar{J}_{2m}(a,\omega_\pm)i'_2(q_\pm r)/D_2(\omega_\pm) -J'_{2m}(r,\omega_\pm)+\Sigma^\pm_{r,2m}(r)q^2_{\rm TF}/q^2_\pm , \tag{B21b}$$

$$\tilde{\Sigma}^\pm_{\theta,2m}(r)=\sigma^\pm_{2m}(r)-C_{2m}S^\pm_{\theta,20}(r) , \tag{B21c}$$

$$\tilde{\Sigma}^\pm_{\phi,21}(r)=\sigma^\pm_{21}(r)-C_{21}S^\pm_{\phi,21}(r) , \tag{B21d}$$

where J_{00S}, J'_{00}, $\bar{J}_{2m}$, D_2, $S^\pm_{\theta,2m}$, and $S^\pm_{\phi,21}$ are defined previously in Eqs. (B8), (B9), and (B10), $\Sigma^\pm_{a,lm}$ are the dimensionless field strengths given in Eqs. (B13), $q_{\rm TF}=\omega_p/\beta$, and

$$2C_{20}=C_{21}=1/q^2_\pm a^2 , \tag{B22a}$$

$$\sigma^\pm_{2m}(r)=n_{2,2m}(r,\omega_\pm)/q_\pm r+\Sigma^\pm_{\theta,2m}(r)q^2_{\rm TF}/q^2_\pm . \tag{B22b}$$

[1]F. Kaczmarek, Acta Phys. Pol. **32**, 1003 (1967); S. Kielich, J. Colloid Interface Sci. **27**, 432 (1968); F. Hache, D. Ricard, C. Flytzanis, and U. Kreibig, Appl. Phys. A **47**, 347 (1988).

[2]D. Stroud and P. M. Hui, Phys. Rev. B **37**, 8719 (1988).

[3]L. Kleinman, Phys. Rev. B **7**, 2288 (1973); A. D. Boardman and M. R. Parker, Phys. Status Solidi B **71** 329 (1975); J. E. Sipe, V. C. Y. So, M. Fukui, and G. I. Stegeman, Phys. Rev. B **21**, 4389 (1980).

[4]X. M. Hua and J. I. Gersten, Phys. Rev. B **33**, 3756 (1986), in their calculation use a circularly polarized light and there is no second-order monopole response.

[5]R. Fuchs and K. L. Kliewer, Phys. Rev. **133**, 2270 (1971).

[6]L. Genzel, T. P. Martin, and U. Kreibig, Z. Phys. B **21**, 339 (1975).

[7]A. Chizmeshya and E. Zaramba, Phys. Rev. B **37**, 2805 (1988).

[8]P. L. Bhatnagar, E. P. Gross, and M. Krook, Phys. Rev. **94**, 511 (1954); A. C. Baynham and A. D. Boardman, *Plasma Effecs in Semiconductors: Helicon and Alfen Waves* (Taylor and Francis, London, 1971); A. D. Baudman and R. Rüppin, Surf. Sci. **112**, 153 (1981); M. H. Cohen, Phys. Rev. **126**, 389 (1962).

[9]A. Ishimaru, *Wave Propagation and Scattering in Random Media* (Academic, New York, 1978), Vol. 2.

[10]U. Kreibig, J. Phys. F **4**, 999 (1974).